RSC Advances

PAPER

View Article Online
View Journal | View Issue

Check for updates

Cite this: *RSC Adv.*, 2019, **9**, 4480

Electrochemical performance of myoglobin based on TiO_2-doped carbon nanofiber decorated electrode and its applications in biosensing†

Yanyan Niu,[a] Hui Xie,[a] Guiling Luo,[a] Wenju Weng,[b] Chengxiang Ruan,*[c] Guangjiu Li[b] and Wei Sun*[ab]

Received 23rd September 2018
Accepted 22nd January 2019

DOI: 10.1039/c8ra07910b

rsc.li/rsc-advances

A new biosensing strategy based on a TiO_2-doped carbon nanofiber (CNF) composite modified electrode was developed. TiO_2@CNF was prepared by electrospinning with further carbonization, before being characterized by various methods and used for electrode modification on the surface of carbon ionic liquid electrode (CILE). Myoglobin (Mb) was further immobilized on the modified electrode surface. The results of ultraviolet-visible (UV-vis) and Fourier transform infrared (FT-IR) spectroscopy showed that Mb maintained its native structure without denaturation in the composite film. Direct electron transfer and the electrocatalytic properties of Mb on the electrode surface were further investigated. A pair of quasi-reversible redox peaks appeared on the cyclic voltammogram, indicating that direct electrochemistry of Mb was realized in the nanocomposite film. This could be attributed to the specific properties of TiO_2@CNF nanocomposite, including a large surface-to-volume ratio, good biocompatibility and high conductivity. Nafion/Mb/TiO_2@CNF/CILE exhibited an excellent electrochemical catalytic ability in the reduction of trichloroacetic acid, $NaNO_2$ and H_2O_2. All results demonstrated potential applications of TiO_2@CNF in third-generation electrochemical biosensors.

1 Introduction

Nanosized titanium dioxide (TiO_2) has been widely used in many fields due to its beneficial properties such as low cost, excellent stability, abundance, and controllable surface structure and geometry, as well as its relatively benign impact on the environment.[1,2] Due to its large specific surface area, good biocompatibility and high hydrophilicity, nanostructured TiO_2 has been used in electrochemical biosensing and electroanalysis. Zhang *et al.* fabricated a plasma polymerization TiO_2@-PPAA (polyacrylic acid) composite and used this as a sensing layer for lysozyme detection with a limit of detection as low as 0.015 ng mL^{-1}.[3] Huo *et al.* prepared an AuNPs/PANI/TiO_2 (gold nanoparticles/polyaniline/TiO_2 nanotube) nanotube composite and used it in assembling immunosensors with a wide linear range and a low detection limit.[4] However, TiO_2 is a wide direct band gap n-type semiconductor with low conductivity and poor catalytic activity, which has considerably limited applications as an efficient electrocatalyst. Interestingly, it is found that a combination of TiO_2 and carbon materials such as carbon nanotubes (CNT), graphene (GR) and carbon nanofibers (CNF) with high conductivity can notably improve the electrical conductivity and electrochemical properties for synergistic effects. These composites were prepared with multiple components by different methods, and exhibited various structures or functions for different applications. Sun *et al.* designed an electrochemical biosensor using hemoglobin immobilized in a chitosan, 1-butyl-3-methylimidazolium hexafluorophosphate ([BMIM]PF_6), TiO_2 and GR nanocomposite-modified glassy carbon electrode.[5] Ahmadalinezhad *et al.* reported carbon-coated TiO_2 nanowires for the acceleration of the interfacial electron transfer rate of enzymes, and used this as a glucose biosensor with high sensitivity and selectivity.[6]

CNF is a one-dimensional (1D) nanomaterial that is more conductive for the effective transmission of electrons along the longitudinal direction.[7] Therefore, CNF could be used in sensors, batteries, supercapacitors, electronic equipment and other fields, offering unique properties. To date, various methods have been used to produce CNFs, with electrospinning considered a desirable method because of its excellent electrical conductivity, large-scale production, good stability and low cost.[8,9] Furthermore, the electrospinning technique is also a simple and flexible way to prepare particle-doped

---

[a] Key Laboratory of Tropical Medicinal Plant Chemistry of Ministry of Education, College of Chemistry and Chemical Engineering, Hainan Normal University, Haikou 571158, P. R. China. E-mail: sunwei@hainnu.edu.cn; Fax: +86 898 31381637; Tel: +86 898 31381637

[b] Key Laboratory of Optic-Electric Sensing and Analytical Chemistry for Life Science of Ministry of Education, College of Chemistry and Molecular Engineering, Qingdao University of Science and Technology, Qingdao 266042, P. R. China

[c] Jiangxi Key Laboratory of Surface Engineering, Jiangxi Science and Technology Normal University, Jiangxi 330013, P. R. China

† Electronic supplementary information (ESI) available. See DOI: 10.1039/c8ra07910b

nanofibers.[10,11] Nanoparticles or soluble inorganic salt precursors can be dispersed in polymer solution to prepare composite nanofibers in the process of electrospinning, then uniform and stable CNFs may be obtained through further carbonization and activation processes. Electrospun CNF is a 1D carbon material, which could also prevent the aggregation of electrochemical active substances and increase the specific surface area.[12,13]

Myoglobin (Mb) is a heme-containing protein present in muscle cells, which is an ideal model of redox proteins for the study of direct electron transfer (DET).[14] In general, the adsorption of redox proteins with redox centers embedded deeply inside the protein structure may denature on the electrode surface.[15] Therefore, the ideal electrode materials and appropriate protein immobilization procedure are very important in research regarding the DET process in redox proteins. The DET process between proteins and electrodes can provide an ideal model for the study of electron transfer mechanisms in real biological systems, and may also play an important role in designing biosensors, biomedical devices and enzymatic bioreactors. Due to the commercial availability and well-documented structure of Mb, studies of DET with Mb have received considerable attention.[16,17] Many methods have been employed to improve the electron transfer efficiency of Mb, such as mediators, promoters or nanomaterials, which open new approaches in the electrochemistry of redox proteins and in applications of biosensors or biocatalysis.

In the present study, TiO_2-doped polyacrylonitrile (PAN) was prepared by electrospinning, and was then subjected to thermal treatment to yield TiO_2-doped carbon nanofiber (TiO_2@CNF). Mb was immobilized on a TiO_2@CNF-modified electrode, and direct electrochemical behaviors between Mb and electrode were discussed. Electrocatalytic behaviors with respect to trichloroacetic acid (TCA), $NaNO_2$ and H_2O_2 at modified electrodes were investigated by cyclic voltammetry. Experimental results showed that this was a suitable, sensitive and selective method for analyte determination. The H_2O_2 content in actual samples such as 3% H_2O_2 disinfectant was further analyzed by the proposed method with satisfactory results.

2 Experimental

2.1 Reagents

PAN (J&K Chemical Co., China), TiO_2 nanoparticles (15–25 nm, Nanjing XFNANO Co., China), graphite powder (average particle size 30 μm, Shanghai Colloid Chemical Co., China), 1-hexylpyridinium hexafluorophosphate ($HPPF_6$; Lanzhou Yulu Fine Chem. Ltd. Co., China), Mb (MW 64500, Sinopharm Chemical Reagent Co., China), Nafion (0.5%, Sigma, USA), TCA (Tianjin Kemiou Chemical Co., China), $NaNO_2$ (Shanghai Chem. Plant, China) and H_2O_2 (Xilong Scientific Ltd. Co., China) were used as provided. 0.1 mol L^{-1} phosphate buffer solutions (PBS) with various pH values were prepared and used as the supporting electrolyte, after being deoxygenized by N_2 for 20 min before each experiment. All other chemicals were of analytical grade and were used without further purification. Doubly distilled water was used throughout the experiments.

2.2 Apparatus

Electrochemical measurements were performed using a CHI 604E electrochemical workstation (Shanghai Chenhua Instrument Co., China). A conventional three-electrode system was used, including a modified electrode as the working electrode, a platinum wire electrode as the auxiliary electrode and a saturated calomel electrode (SCE) as the reference electrode. Ultraviolet-visible (UV-vis) absorption spectra and Fourier transform infrared (FT-IR) spectra were recorded on a UV 5 ultraviolet-visible spectrophotometer (Mettler Toledo, America) and Tensor 27 FT-IR spectrophotometer (Bruker, Germany), respectively. Scanning electron microscopy (SEM) and transmission electron microscopy (TEM) were obtained on a JSM-7600F (JEOL, Japan) scanning electron microscope and JEM-2010F (JEOL, Japan) transmission electron microscope, respectively. X-ray diffraction (XRD) experiments were performed on a D/Max-2500 V X-ray diffractometer (Rigaku, Japan) with Cu-Kα radiation. Raman spectra were obtained on a LabRAM HR system using 532 nm lasers (Horiba, France). X-ray photoelectron spectroscopy (XPS) was carried on an AXIS HIS 165 spectrophotometer (Kratos Analytical, UK).

2.3 Preparation of TiO_2@CNF nanocomposite

Electrospinning was used to fabricate TiO_2@CNF nanocomposite *via* the following procedure. First, 0.3 g TiO_2 nanoparticle and 0.5 g PAN were dissolved in 9.5 g dimethylformamide (DMF) with vigorous stirring at room temperature for 12 h to form a stable and homogenous solution. Electrospinning apparatus was laboratory-built with a high-voltage power supply. The TiO_2–PAN–DMF mixed solution was loaded into a 5 mL syringe with a stainless-steel needle. The tip of the syringe needle was connected to the positive terminal of the high-voltage power supply, while the collector was clamped to the negative terminal. The distance between the needle tip and the collector was 18 cm, and the applied high voltage was 18 kV *via* a direct current supply. The mixed solution was pushed at a rate of 0.5 mL h^{-1} using a syringe pump. The electrospinning process was then performed at room temperature, and the nanofiber was collected on a roller collector wrapped in aluminum foil. Finally, the as-prepared TiO_2@PAN nanofiber was peeled off from the collector. TiO_2@CNF nanocomposite was prepared from the above TiO_2@PAN nanofiber *via* thermal treatments calcining at 800 °C for 2 h under an N_2 atmosphere. After being cooled to room temperature, TiO_2@CNF nanocomposite was obtained and used directly.

2.4 Preparation of Nafion/Mb/TiO_2@CNF/CILE

Ionic liquid (IL)-modified carbon paste electrode (CILE) was prepared on the basis of a previously reported procedure[18] with $HPPF_6$ and graphite powder (mass ratio of 1 : 2). Then, the CILE surface was gently smoothed on a piece of weighing paper just before use.

The modified electrode was prepared with following procedure: 8.0 μL of 1.5 mg mL^{-1} TiO_2@CNF suspension solution was casted onto the CILE surface and left to dry at room temperature (TiO_2@CNF/CILE). Then, 8.0 μL of 15 mg mL^{-1} Mb water solution was dropped onto the surface of TiO_2@CNF/CILE and allowed to dry at room temperature to obtain Mb/TiO_2@CNF/CILE. Finally, 6.0 μL of 0.5% Nafion solution was spread onto the surface of Mb/TiO_2@CNF/CILE to obtain Nafion/Mb/TiO_2@CNF/CILE, which was used as the working electrode. Other electrodes such as Nafion/TiO_2@CNF/CILE, Nafion/Mb/CILE and Nafion/CILE were prepared using a similar procedure. These modified electrodes were stored at 4 °C in a refrigerator while not in use.

3 Results and discussion

3.1 Characterization of TiO_2@CNF nanocomposite

SEM patterns of TiO_2@CNF nanocomposite are shown in Fig. 1A and B, which suggest that the products maintained a good fibrous morphology after carbonization at high temperature. These nanofibers were uniform, with a diameter in the range of ∼500–1000 nm, and could form a three-dimensional (3D) network structure. As observed in Fig. 1B, the high magnification of the SEM findings showed many small nano-protrusions covered and dotted on the surface of the nanofibers, which was ascribed to the presence of TiO_2 nanoparticles. Therefore, it was more beneficial to increase the roughness and specific surface area of the nanofiber. The high-resolution TEM images of TiO_2@CNF nanocomposite were recorded with different magnitudes, and the results are shown in Fig. 1C and D, showing a typical *in situ* structure of spherical TiO_2 nanoparticles that were distributed uniformly on and inside CNF. As shown in Fig. 1D, TiO_2 nanoparticles were wrapped by several graphitized carbon layers such as nanoparticles/graphite core–shell microstructures. Furthermore, clear lattice fringes of graphite carbon could be observed in Fig. 1E, indicating the successful preparation of the TiO_2-doped CNF.

The XRD pattern of the nanocomposite further reflected an amorphous feature with characteristic diffraction peaks of the anatase phase and graphite carbon (Fig. 1F), indicating no obvious impurity.[19] XPS analysis of TiO_2@CNF nanocomposite displayed peaks at around 531 eV and 284 eV, which corresponded to O_{1s} and C_{1s}, respectively. The symmetrical XPS peak of O_{1s} (Fig. 1G) could belong to the lattice oxygen (531 eV) in the TiO_2 crystal structure, and the XPS peak of C_{1s} (Fig. 1H) at 284 eV belonged to the graphitization structure of CNF. Raman spectra of TiO_2@CNF nanocomposite (Fig. 1I) were recorded by employing 532 nm excitation, with two broad and weak peaks

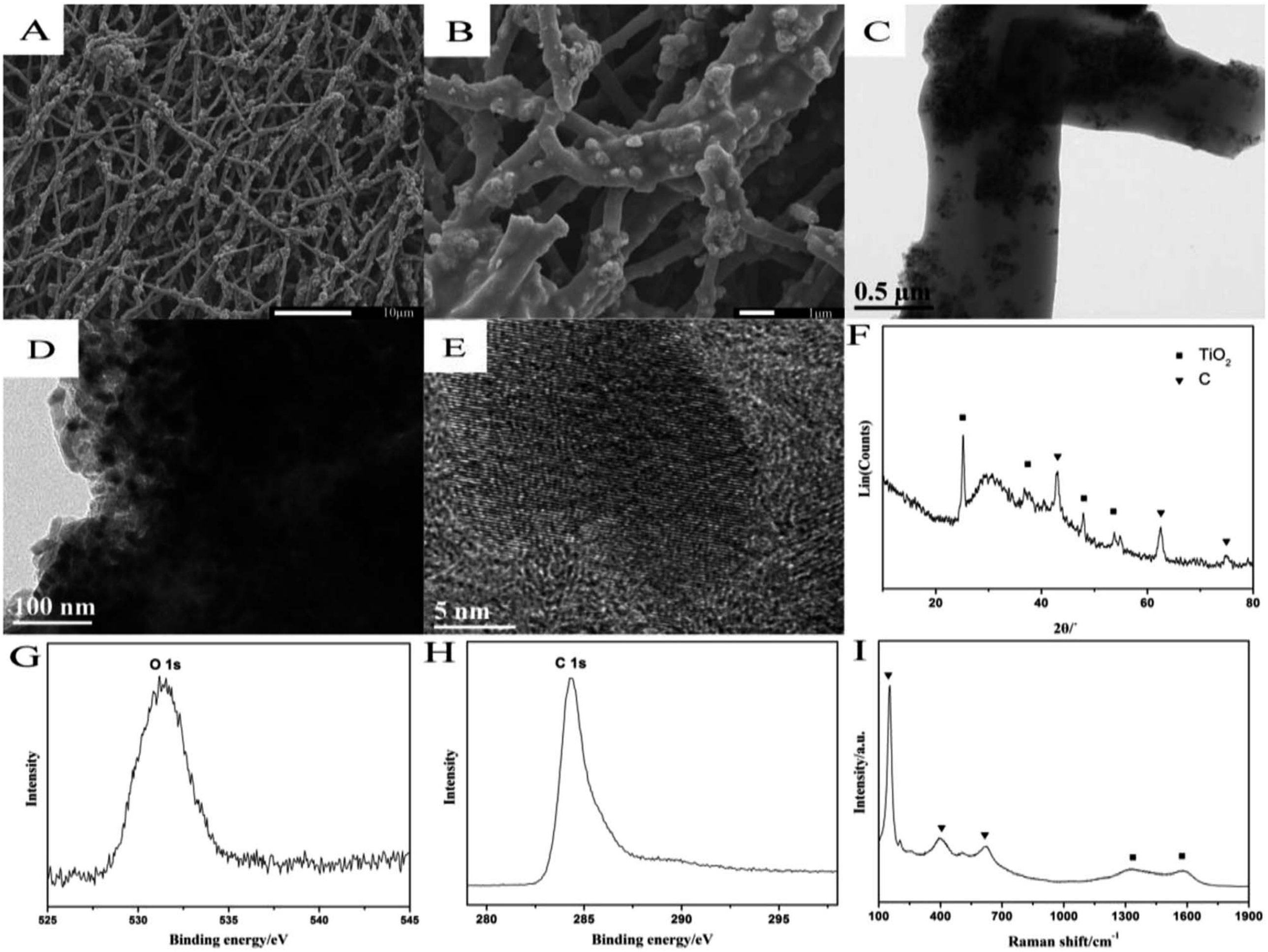

Fig. 1 Characterization of TiO_2@CNF nanocomposite: (A and B) SEM images; (C–E) TEM images; (F) XRD pattern; (G and H) XPS spectra and (I) Raman spectra.

appearing at 1336.49 cm^{-1} and 1575.36 cm^{-1}. The peaks represented D and G bands caused by the vibration mode (E_{2g}) corresponding to the disordered structure of CNF (such as lattice defects, amorphous carbon impurities *etc.*), and the high symmetrical and directional structure of graphite, respectively.[20] Meanwhile, one strong peak at 146.53 cm^{-1} and two weak peaks at 401.85 and 631.89 cm^{-1} corresponded to the E_g, B_{1g} and E_g vibration mode of anatase phase TiO_2, which were consistent with those of XRD and XPS.

3.2 Spectroscopic investigations

UV-vis absorption spectrophotometry may be used to probe the typical secondary structure of a protein through the migration or disappearance of Soret absorption bands.[21] As shown in Fig. S1 (ESI†), the similar spectroscopic position indicated that Mb retained its native structure after mixing with TiO_2@CNF, which may be attributed to the good biocompatibility of TiO_2@CNF nanocomposite. FT-IR spectroscopy was further employed, and the results are shown in Fig. S2 (ESI†), with similar FT-IR spectra which also indicated that the Mb molecule retained its natural conformation after mixing with TiO_2@CNF nanocomposite. Further, the oxygen vacancy defects and surface crystal defects of TiO_2 on the surface of CNF could influence the interaction of Mb with CNF.[22,23]

3.3 Characterization of the modified electrodes

Direct electrochemical behaviors of Mb were evaluated by cyclic voltammetry with different modified electrodes in pH 4.0 PBS. As shown in Fig. 2A, on Nafion/CILE (curve a) and Nafion/TiO_2@CNF/CILE (curve b), no notable electrochemical response could be detected, indicating the presence of no electroactive substances. The increase of background current on Nafion/TiO_2@CNF/CILE demonstrated that TiO_2@CNF nanocomposite on the electrode surface with the 3D network increased the interfacial roughness and the charging peak current. On Nafion/Mb/CILE (curve c), a pair of redox peaks appeared, which revealed the realization of DET between Mb and CILE. While on Nafion/Mb/TiO_2@CNF/CILE (curve d), the redox peak currents increased greatly, which was due to the presence of TiO_2@CNF nanocomposite on the electrode with a long fiber structure, good biocompatibility and a high conductivity surface that promoted the electron transfer rate. The formal peak potential ($E^{O\prime}$; the midpoint between the reduction and oxidation peak) was recorded as −0.24 V and the ratio of the redox peak current (I_{pc}/I_{pa}) was 1.32, indicating a quasi-reversible electrochemical process.

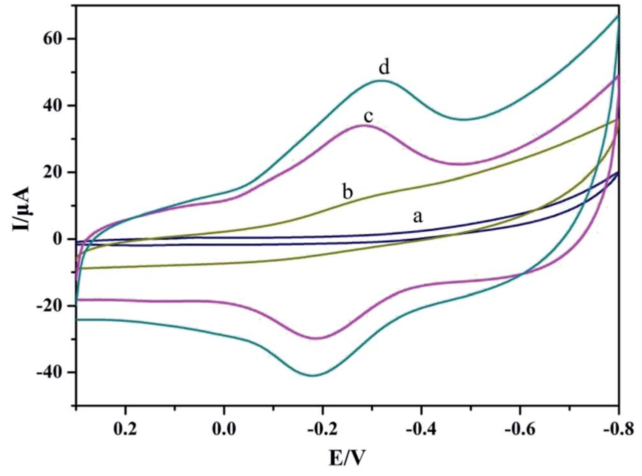

Fig. 2 Cyclic voltammograms of Nafion/CILE (curve a), Nafion/TiO_2@CNF/CILE (curve b), Nafion/Mb/CILE (curve c) and Nafion/Mb/TiO_2@CNF/CILE (curve d) in pH 4.0 PBS with a scan rate of 100 mV s^{-1}.

Electrochemical impedance spectroscopy (EIS) is commonly used to obtain information about the modified electrode during the modification process.[24] Fig. S3 (ESI†) showed the EIS of different modified electrodes, and the changes in electron transfer resistance (R_{et}) values indicated that Mb had been successfully immobilized on the electrode surface. After TiO_2@CNF nanocomposite was modified on the surface of the electrode, the interfacial resistance was greatly decreased due to the high conductivity of CNF.

3.4 Cyclic voltammetric studies

The pH effect of the supporting electrolyte on the redox peak responses of Mb was investigated. Fig. 3A shows typical CVs of Nafion/Mb/TiO_2@CNF/CILE in pH ∼3.0–8.0 PBS. Nearly reversible voltammograms with stable and well-defined redox peaks were obtained, and the potential of redox peaks shifted negatively with the increase of pH. The $E^{O\prime}$ had a linear relationship with pH value and the slope value was 53.96 mV pH^{-1}, which was a little smaller than the theoretical value (59 mV pH^{-1}) for a single-proton coupled reversible one-electron transfer process.[25,26] The reason for this might be the influence of the protonation states of transligands to the heme iron and amino acids around the heme, or the protonation of the water molecule coordinated to the central iron.[27,28] $E^{O\prime}$ was between the reported values of Mb direct electrochemistry, such as −0.15 V (*vs.* SCE, pH 3.0),[29] −0.18 V (*vs.* SCE, pH 3.0)[30] and −0.09 V (*vs.* SCE, pH 3.0).[31] Furthermore, the negative shift of $E^{O\prime}$ was indicative of the involvement of H^+ in the electrode reaction.[14] Therefore, the electrochemical reaction of Mb could be expressed as: $\text{Mb–Fe(III)} + H^+ + e^- \leftrightarrow \text{Mb–Fe(II)}$,[14,21] which indicated the reduction of Mb–Fe(III) to Mb–Fe(II) on the forward scan and reoxidation to Mb–Fe(III) on the reverse scan. In pH 4.0 buffer, the largest redox peak current appeared, which was chosen as the optimum pH for determination.

The influence of scan rate on cyclic voltammetric responses of Nafion/Mb/TiO_2@CNF/CILE in pH 4.0 PBS was further recorded, and the results are shown in Fig. 3B. Well-defined and symmetric redox peaks appeared in a scan rate range from 50 to 1000 mV s^{-1}, in which the redox peak currents and the peak-to-peak separation increased. Two linear regression equations were calculated as I_{pc} (μA) = 93.23ν (V s^{-1}) + 4.28 ($R = 0.9914$) and I_{pa} (μA) = −63.90ν (V s^{-1}) − 1.60 ($R = 0.9921$), respectively, indicating a characteristic surface-confined thin-layer electrochemical process. The average surface concentration of electroactive Mb (Γ^*, mol cm^{-2}) could be estimated from the charge integration of the reduction peak based on the Faraday equation: $Q = nFA\Gamma^*$,[32] where F is the Faraday constant, Q is the

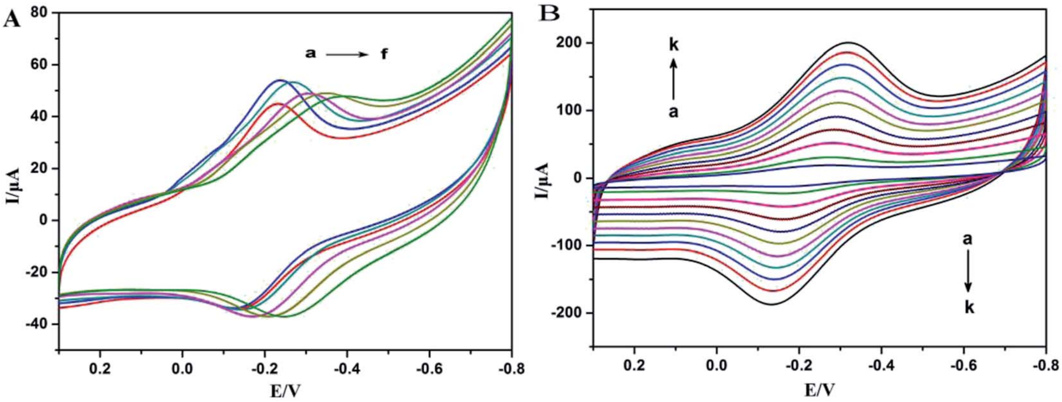

Fig. 3 (A) Cyclic voltammograms of Nafion/Mb/TiO_2@CNF/CILE at different pH (curves a → f: 3.0, 4.0, 5.0, 6.0, 7.0, 8.0) with a scan rate of 100 mV s^{-1}. (B) Cyclic voltammograms of Nafion/Mb/TiO_2@CNF/CILE at different scan rates (curves a → k: 50, 100, 200, 300, 400, 500, 600, 700, 800, 900, 1000 mV s^{-1}) in pH 4.0 PBS.

charge by integrating the reduction peak of Mb, and n and A represent the number of electrons transferred and the geometrical surface area of the electrode, respectively. The number of electroactive Mb molecules was estimated to be 4.69 $\times 10^{-10}$ mol cm^{-2}, accounting for 8.20% of the total Mb on the electrode surface (5.72×10^{-9} mol cm^{-2}). Therefore, Mb molecules in the inner layers close to the electrode surface with a suitable orientation can exchange electrons with the electrode more effectively.[15,21] The relationships of E_p with $\ln \nu$ were constructed with two straight lines as E_{pa} (V) = 0.058 ln ν (V s^{-1}) − 0.12 ($R = 0.9890$) and E_{pc} (V) = −0.052 ln ν (V s^{-1}) − 0.30 ($R = 0.9955$). According to the model of Laviron's equation,[33] the values of the electron transfer coefficient (α), electron transfer number (n) and the heterogeneous electron transfer constants (k_s) were estimated as 0.53, 0.93 and 1.81 s^{-1}, respectively.

3.5 Electrocatalytic properties

Redox protein-modified electrodes exhibit good electrocatalytic activity for various substances due to their mimic peroxidase activity with more specificity. TCA is an important monitoring target for environmental analysis due to the wide usage of herbicides and preservatives. Therefore, rapid and sensitive detection of TCA has become an important research target. TCA is difficult to degrade electrocatalytically on the surface of an ordinary electrode due to its good stability, while the redox protein-modified electrode can reduce the activation energy and accelerate the rate of electrocatalytic reduction.

The electrocatalytic reduction of TCA at Nafion/Mb/TiO_2@CNF/CILE in pH 4.0 PBS was investigated by cyclic voltammetry. As shown in Fig. 4A, an obvious increase of the reduction peak current at −0.28 V was observed with increments of TCA concentration accompanied by a decrease in the oxidation peak current, which are characteristic of the electrochemical catalysis of TCA. The process could be described in terms of the following proposed reaction:[34,35]

$$\text{Mb–Fe(III)} + H^+ + e^- \rightarrow \text{Mb–Fe(II)}$$

$$\text{2Mb–Fe(II)} + Cl_3CCOOH + H^+ \rightarrow \text{2Mb–Fe(III)} + Cl_2CHCOOH + Cl^-$$

A linear relationship between the catalytic reduction peak current and the concentration of TCA was obtained in the concentration range of 5.0 to 105.0 mmol L^{-1} (inset in Fig. 4A), with the calibration equation as I (μA) = 1.49C (mmol L^{-1}) − 1.73 ($R = 0.9961$) and the detection limit of 1.6 mmol L^{-1} (3σ). While the TCA concentration was more than 105.0 mmol L^{-1},

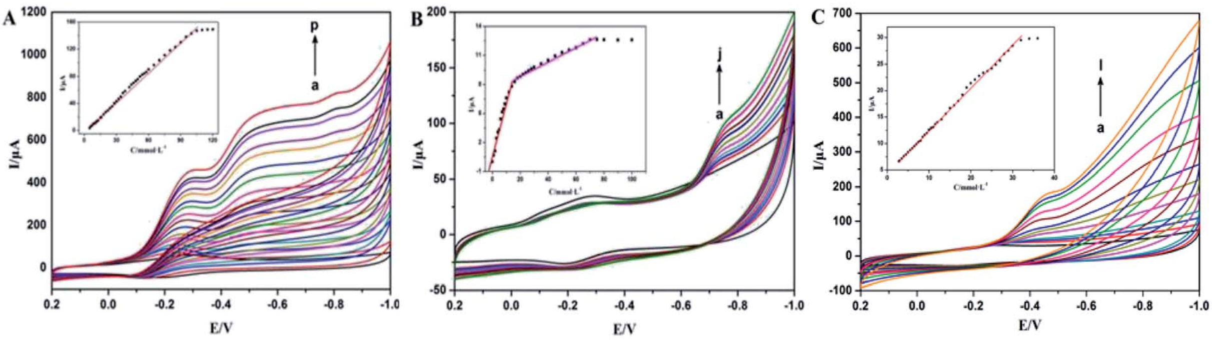

Fig. 4 Cyclic voltammograms of Nafion/Mb/TiO_2@CNF/CILE in pH 4.0 PBS in the presence of (A) 0, 3, 6, 10, 15, 20, 26, 32, 38, 44, 50, 60, 70, 80, 90, 105 mmol L^{-1} TCA (curves a to p, inset is the linear relationship of catalytic reduction peak currents *vs.* TCA concentration); (B) 0, 6, 9, 12, 20, 30, 40, 50, 60, 70 mmol L^{-1} $NaNO_2$ (curves a to j, inset is the linear relationship of catalytic reduction peak currents *vs.* $NaNO_2$ concentration); (C) 0, 1, 2, 3, 5, 7, 10, 15, 20, 25, 30, 32 mmol L^{-1} H_2O_2 (curves a to l, inset is the linear relationship of the catalytic reduction peak currents *vs.* H_2O_2 concentration).

Table 1 Detection results of H_2O_2 content in disinfectant samples (n = 3)

Sample	Labeled (mmol L^{-1})	Detected (mmol L^{-1})	Added (mmol L^{-1})	Total (mmol L^{-1})	Recovery (%)
3% H_2O_2 disinfectant	8.82	9.11	1.00	10.17	106.00
			2.00	10.99	94.00
			3.00	12.31	106.67

the reduction peak current tended to be stable, which conformed to a typical Michaelis–Menten kinetic mechanism. On the basis of the equation $1/I_{ss} = (1/I_{max})(1 + K_M^{app}/C)$, where I_{ss} is the stable current with the addition of the substrate, C is the bulk concentration of the substrate, and I_{max} represents the maximum current measured *via* the saturated substrate condition,[36] the value of the apparent Michaelis–Menten constant (K_M^{app}) could be calculated as 5.06 mmol L^{-1}.

$NaNO_2$ is widely used in industry and food processing and can be transformed into carcinogen nitrosamines in the human body. The electrocatalytic reduction of $NaNO_2$ was investigated by cyclic voltammetry in pH 4.0 PBS, with the curves shown in Fig. 4B. The reduction peak current increased clearly at −0.75 V with increasing concentration of $NaNO_2$, and was accompanied by a decrease in the oxidation peak current. The catalytic reduction peak current was linear with $NaNO_2$ concentration in the range from ∼1.0–14.0 mmol L^{-1} and ∼14.0–70.0 mmol L^{-1}, with the linear regression equations as I (μA) = 0.59C (mmol L^{-1}) + 0.45 (n = 13, R = 0.9670) and I (μA) = 0.076C (mmol L^{-1}) + 7.40 (n = 16, R = 0.9905). The detection limit was obtained as 0.3 mmol L^{-1} (3σ).

Fig. 4C shows a plot of the variation in electrocatalytic current against H_2O_2 concentration in pH 4.0 PBS. Along with increasing H_2O_2 concentration from 2.8 to 32.0 mmol L^{-1}, reduction peak current shifted negatively to −0.42 V and increased linearly with the linear regression equation as I (μA) = 0.81C (mmol L^{-1}) + 4.39 (R = 0.9976) and the detection limit was 1.0 mmol L^{-1} (3σ). Meanwhile, the oxidation peak current decreased gradually and finally disappeared, indicating a typical electrocatalytic process.

Control experiments were performed for comparison, in which other modified electrodes were used including Nafion/CILE, Nafion/TiO_2@CNF/CILE and Nafion/Mb/CILE for the electroreduction of these targets. From the results shown in Fig. S5 (ESI†), it can be seen that Nafion/CILE and Nafion/TiO_2@CNF/CILE exhibited no effects on the electroreduction of analytes without the appearance of the redox peaks. On Nafion/Mb/CILE, the electrocatalytic effects could be observed with small responses, which could be ascribed to the presence of Mb on the electrode surface. Mb exhibits peroxidase activity, and the Mb-modified electrode can catalyze the reduction of specific analytes. TiO_2@CNF on the electrode surface acts as a fast electron transfer bridge for the DET process of Mb. Therefore, in the absence of TiO_2@CNF on the modified electrode, the enhancement of the electron transfer rate was not obvious and the electrocatalytic currents were significantly smaller than that of Nafion/Mb/TiO_2@CNF/CILE.

3.6 Sample detection

To evaluate the practical analytical applications of Nafion/Mb/TiO_2@CNF/CILE for H_2O_2 detection, 3% H_2O_2 disinfectant (Guangdong Nanguo Pharmaceutical Ltd. Co., China) was used as a real sample, and was diluted 100 times and tested with cyclic voltammetry. As shown in Table 1, the detection result was close to the labeled value and the recovery test was checked by the standard addition method with data in the range 94.00–106.67%, demonstrating that this Mb-based electrochemical sensor was appropriate for the detection of the practical H_2O_2 samples.

4 Conclusion

In this paper, TiO_2@CNF nanocomposites were successfully prepared by electrospun TiO_2-doped PAN as an inexpensive precursor under controlled synthesis conditions, and were calcined *via* a one-step heat treatment. Furthermore, TiO_2@CNF possessed biocompatible and conductive properties, which were applied to fabricate an electrochemical sensor with Mb and Nafion. Spectroscopic data suggested that Mb retained its native structure. The modified electrode acted as an excellent platform for realizing the direct electrochemistry of Mb with quasi-reversible surface-controlled electron transfer process. The immobilized Mb displayed excellent electrocatalytic behavior toward various substances including TCA, $NaNO_2$ and H_2O_2 with wider linear ranges and a low detection limit. These results illustrate that TiO_2@CNF has potential applications in the fabrication of third-generation, reagent-less electrochemical biosensors.

Conflicts of interest

There are no conflicts to declare.

Acknowledgements

This project was support by the Hainan Provincial National Natural Science Foundation of China (2017CXTD007), the National Natural Science Foundation of China (21665007, 51363008), the Program for Innovative Research Team in University (IRT-16R19), the Key Science and Technology Program of Haikou City (2017042), the Foundation of Key Laboratory of Optic-Electric Sensing and Analytical Chemistry for Life Science at the Ministry of Education at Qingdao University of Science and Technology (STAM201808), and the China Scholarship Council (1804250008, award to Chengxiang Ruan for 1 year's study abroad at North Dakota State University).

References

1 J. H. Li, D. Z. Kuang, Y. L. Feng and M. Q. Liu, Voltammetric determination of *o*-phenylenediamine in industrial

wastewater by an electrode modified with nanocomposite film of TiO_2/hydroxyapatite/MWCNT, *Chin. J. Anal. Chem.*, 2011, **39**, 1864–1870.

2 D. Hassen, M. A. Shenashen, S. A. El-Safty, M. M. Selim, H. Isago, A. Elmarakbi, A. El-Safty and H. Yamaguchi, Nitrogen-doped carbon-embedded TiO_2 nanofibers as promising oxygen reduction reaction electrocatalysts, *J. Power Sources*, 2016, **330**, 292–303.

3 Z. H. Zhang, S. Zhang, L. H. He, D. L. Peng, F. F. Yan, M. H. Wang, J. H. Zhao, H. Z. Zhang and S. M. Fang, Feasible electrochemical biosensor based on plasma polymerization-assisted composite of polyacrylic acid and hollow TiO_2 spheres for sensitively detecting lysozyme, *Biosens. Bioelectron.*, 2015, **74**, 384–390.

4 X. H. Huo, P. P. Liu, J. Zhu, X. Q. Liu and H. X. Ju, Electrochemical immunosensor constructed using TiO_2 nanotubes as immobilization scaffold and tracing tag, *Biosens. Bioelectron.*, 2016, **85**, 698–706.

5 J. Y. Sun, K. J. Huang, S. F. Zhao, Y. Fan and Z. W. Wu, Direct electrochemistry and electrocatalysis of hemoglobin on chitosan-room temperature ionic liquid-TiO_2-graphene nanocomposite film modified electrode, *Bioelectrochemistry*, 2011, **82**, 125–130.

6 A. Ahmadalinezhad, G. S. Wu, W. Keeler and A. C. Chen, Fabrication and electrochemical study of carbon modified TiO_2 nanowires, *Electrochem. Commun.*, 2014, **49**, 25–29.

7 J. L. Xu, L. Zhang, G. C. Xu, Z. P. Sun, C. Zhang, X. Ma, C. L. Qi, L. Zhang and D. Z. Jia, Facile synthesis of NiS anchored carbon nanofibers for high-performance supercapacitors, *Appl. Surf. Sci.*, 2018, **434**, 112–119.

8 Y. Li, W. Ou-Yang, X. Xu, M. Wang, S. Hou, T. Lu, Y. Yao and L. Pan, Micro/mesoporous carbon nanofibers embedded with ordered carbon for flexible supercapacitors, *Electrochim. Acta*, 2018, **271**, 591–598.

9 G. Y. Oh, Y. W. Ju, H. R. Jung and W. J. Lee, Preparation of the novel manganese-embedded PAN-based activated carbon nanofibers by electrospinning and their toluene adsorption, *J. Anal. Appl. Pyrolysis*, 2008, **81**, 211–217.

10 C. A. Bonino, L. Ji, Z. Lin, O. Toprakci, X. Zhang and S. A. Khan, Electrospun carbon-tin oxide composite nanofibers for use as lithium ion battery anodes, *ACS Appl. Mater. Interfaces*, 2011, **3**, 2534–2542.

11 I. Meschini, F. Nobili, M. Mancini, R. Marassi, R. Tossici, A. Savoini, M. L. Focarete and F. Croce, High-performance Sn@carbon nanocomposite anode for lithium batteries, *J. Power Sources*, 2013, **226**, 241–248.

12 Z. Li, J. W. Zhang, J. Shu, J. P. Chen, C. H. Gong, J. H. Guo and L. G. Yu, Carbon nanofibers with highly dispersed tin and tin antimonide nanoparticles: preparation *via* electrospinning and application as the anode materials for lithium-ion batteries, *J. Power Sources*, 2018, **381**, 1–7.

13 J. W. Jung, C. L. Lee, S. Yu and I. D. Kim, Electrospun nanofibers as a platform for advanced secondary batteries: a comprehensive review, *J. Mater. Chem.*, 2016, **4**, 703–750.

14 G. Y. Chen, H. Sun and S. F. Hou, Electrochemistry and electrocatalysis of myoglobin immobilized in sulfonated graphene oxide and Nafion films, *Anal. Biochem.*, 2016, **502**, 43–49.

15 S. F. Wang, F. Xie and G. D. Liu, Direct electrochemistry and electrocatalysis of heme proteins on SWCNTs-CTAB modified electrodes, *Talanta*, 2009, **77**, 1343–1350.

16 T. Wang, L. Wang, J. J. Tu, H. Y. Xiong and S. F. Wang, Direct electrochemistry and electrocatalysis of heme proteins immobilised in carbon-coated nickel magnetic nanoparticle-chitosan-dimethylformamide composite films in room-temperature ionic liquids, *Bioelectrochemistry*, 2013, **94**, 94–99.

17 C. X. Ruan, T. T. Li, Q. J. Niu, M. Lu, J. Lou, W. M. Gao and W. Sun, Electrochemical myoglobin biosensor based on graphene-ionic liquid-chitosan bionanocomposites: direct electrochemistry and electrocatalysis, *Electrochim. Acta*, 2012, **64**, 183–189.

18 X. L. Niu, L. J. Yan, X. B. Li, A. H. Hu, C. J. Zheng, Y. L. Zhang and W. Sun, Sensitive voltammetric detection of metal with a TiO_2 nanowire modified carbon ionic liquid electrode, *Int. J. Electrochem. Sci.*, 2016, **11**, 1720–1729.

19 Z. Z. Li, X. L. Cui, J. S. Zheng and Q. F. Wang, Photoelectrochemical properties of TiO_2 coated on carbon nanofibers with different microstructure film electrodes, *Chem. Res. Chin. Univ.*, 2008, **29**, 1195–1199.

20 D. F. Li, H. J. Wang and X. K. Wang, Raman spectra of PAN-based carbon fibers during graphitization, *Spectrosc. Spectral Anal.*, 2007, **27**, 2249–2253.

21 F. Shi, W. C. Wang, S. X. Gong, B. X. Lei, G. J. Li, X. M. Lin, Z. F. Sun and W. Sun, Application of titanium dioxide nanowires for the direct electrochemistry of hemoglobin and electrocatalysis, *J. Chin. Chem. Soc.*, 2015, **62**, 554–561.

22 D. S. Kong, H. Y. Liu, E. J. Fan, W. H. Lv, Z. Y. Yu and Y. Y. Feng, Electrochemical studies on the ionic charge transfer properties of the oxygen vacancy defects in the oxide films formed on titanium, *Electrochemistry*, 2009, **15**, 320–325.

23 P. Xiao, Y. H. Zhang and G. Z. Cao, Effect of surface defects on biosensing properties of TiO_2 nanotube arrays, *Sens. Actuators, B*, 2011, **155**, 159–164.

24 Z. H. Zhu, X. Li, Y. Wang, Y. Zeng, W. Sun and X. T. Huang, Direct electrochemistry and electrocatalysis of horseradish peroxidase with hyaluronic acid-ionic liquid-cadmium sulfide nanorod composite material, *Anal. Chim. Acta*, 2010, **670**, 51–56.

25 A. M. Bond, *Modern polarographic methods in analytical chemistry*, Marcel Dekker, New York, 1980.

26 L. Meites, *Polarographic techniques*, Wiley, New York, 1965.

27 I. Yamazaki, T. Araiso, Y. H. Ayashi, H. Yamada and R. Makino, Analysis of acid-base properties of peroxidase and myoglobin, *Adv. Biophys.*, 1978, **11**, 249–281.

28 D. P. Qian, W. B. Li, F. T. Chen, Y. Huang, N. Bao, H. Y. Gu and C. M. Yu, Voltammetric sensor for trichloroacetic acid using a glassy carbon electrode modified with Au@Ag nanorods and hemoglobin, *Microchim. Acta*, 2017, **184**, 1977–1985.

29 X. L. Wang, L. H. Liu, W. Zheng, W. Chen, G. J. Li and W. Sun, Electrochemical behaviors of myoglobin on

graphene and Bi film modified electrode and electrocatalysis to trichloroacetic acid, *Int. J. Electrochem. Sci.*, 2016, **11**, 1821–1830.

30 F. Shi, J. W. Xi, F. Hou, L. Han, G. J. Li, S. X. Gong, C. X. Chen and W. Sun, Application of three-dimensional reduced graphene oxide-gold composite modified electrode for direct electrochemistry and electrocatalysis of myoglobin, *Mater. Sci. Eng., C*, 2016, **58**, 450–457.

31 X. L. Niu, Z. R. Wen, X. Y. Li, L. J. Yan, W. L. Zhang, S. X. Gong, Z. F. Shi and W. Sun, Direct electrochemistry of myoglobin on three-dimensional graphene-nickel oxide modified electrode and electrocatalytic detection of trichloroacetic acid, *Curr. Anal. Chem.*, 2017, **13**, 410–416.

32 W. Sun, Y. Q. Guo, T. T. Li, X. M. Ju, J. Lou and C. X. Ruan, Electrochemistry of horseradish peroxidase entrapped in graphene and dsDNA composite modified carbon ionic liquid electrode, *Electrochim. Acta*, 2012, **75**, 381–386.

33 E. Laviron, General expression of the linear potential sweep voltammogram in the case of diffusionless electrochemical systems, *J. Electroanal. Chem.*, 1979, **101**, 19–28.

34 X. S. Yang, X. Chen, X. Zhang, W. S. Yang and D. G. Evans, Direct electrochemistry and electrocatalysis with horseradish peroxidase immobilized in polyquaternium-manganese oxide nanosheet nanocomposite films, *Sens. Actuators, B*, 2008, **134**, 182–188.

35 W. Sun, X. Q. Li and K. Jiao, Direct electrochemistry of myoglobin in a Nafion-ionic liquid composite film modified carbon ionic liquid electrode, *Electroanalysis*, 2009, **21**, 959–964.

36 R. A. Kamin and G. S. Wilson, Rotating ring-disk enzyme electrode for biocatalysis kinetic studies and characterization of the immobilized enzyme layer, *Anal. Chem.*, 1980, **52**, 1198–1205.